

## High-Resolution Rainfall Maps from Commercial Microwave Links for a Data-Scarce Region in West Africa

MOUMOUNI DJIBO,<sup>a,b,c</sup> CHRISTIAN CHWALA,<sup>a,c</sup> MAXIMILIAN GRAF,<sup>a,c</sup> JULIUS POLZ,<sup>c</sup> HARALD KUNSTMANN,<sup>a,c</sup> AND FRANÇOIS ZOUGMORE<sup>b</sup>

<sup>a</sup> *Institute of Geography, University of Augsburg, Augsburg, Germany*

<sup>b</sup> *Laboratoire de Matériaux et Environnement, Université Joseph KI-ZERBO, Ouagadougou, Burkina Faso*

<sup>c</sup> *Institute of Meteorology and Climate Research, Karlsruhe Institute of Technology, Garmisch-Partenkirchen, Germany*

(Manuscript received 1 February 2023, in final form 21 July 2023, accepted 26 July 2023)

**ABSTRACT:** We present high-resolution rainfall maps from commercial microwave link (CML) data in the city of Ouagadougou, Burkina Faso. Rainfall was quantified based on data from 100 CMLs along unique paths and interpolated to achieve rainfall maps with a 5-min temporal and 0.55-km spatial resolution for the monsoon season of 2020. Established processing methods were combined with newly developed filtering methods, minimizing the loss of data availability. The rainfall maps were analyzed qualitatively both at a 5-min and aggregated daily scales. We observed high spatiotemporal variability on the 5-min scale that cannot be captured with any existing measurement infrastructure in West Africa. For the quantitative evaluation, only one rain gauge with a daily resolution was available. Comparing the gauge data with the corresponding CML rainfall map pixel showed a high agreement, with a Pearson correlation coefficient  $> 0.95$  and an underestimation of the CML rainfall maps of  $\sim 10\%$ . Because the CMLs closest to the gauge have the largest influence on the map pixel at the gauge location, we thinned out the CML network around the rain gauge synthetically in several steps and repeated the interpolation. The performance of these rainfall maps dropped only when a radius of 5 km was reached and approximately one-half of all CMLs were removed. We further compared ERA5 and GPM IMERG data with the rain gauge and found that they had much lower correlation than data from the CML rainfall maps. This clearly highlights the large benefit that CML data can provide in the data-scarce but densely populated African cities.

**SIGNIFICANCE STATEMENT:** In this study, we investigate the possibility of deriving accurate high-resolution rainfall maps from commercial microwave link (CML) data in West Africa. The main challenges are the lack of reference data in this area and the adoption of existing processing tools without reference data. We show CML rainfall maps for Ouagadougou, Burkina Faso, with a resolution of 5 min and 0.55 km, which is unprecedented in this region. The comparison with the only available rain gauge, which provides data only at a daily resolution, yields a Pearson correlation of  $> 0.95$ . An analysis of synthetically thinned-out networks shows that this accuracy is valid for the whole domain. Comparing reanalysis and satellite data with the rain gauge and CML data showed a poor performance of these gridded reference datasets. Also, a high coincidence of temporal dynamics between CML rainfall maps and satellite products was observed. Overall, these findings support the potential of CMLs for future hydrometeorological applications in West Africa.

**KEYWORDS:** Africa; Rainfall; Gauges; Microwave observations; Remote sensing


### 1. Introduction

Extreme weather and climate events, such as heat waves, heavy rainfall, and floods, are becoming progressively more severe as global warming increases (Fischer and Knutti 2015). Burkina Faso, like most African countries, is subject to these negative effects of climate change and hydrometeorological extremes, which are a severe threat to the country because it heavily depends on agriculture (Tomalka et al. 2021). Therefore, the management of water resources and natural disasters is vital for Burkina Faso. However, 60% of Africa does not

have access to early warning systems and climate information services, due to a lack of systematic observations (UNFCCC 2022). Especially, missing rainfall information hampers water management and, in consequence, also the adaptation and resilience against climate change impacts.

To date, two sources of rainfall information are available in Burkina Faso: rain gauges and satellite observations. Bliefert et al. (2021) collected rainfall data from West Africa and found that the Agence Nationale de la Météorologie (ANAM) operated up to 130 rainfall stations during the 1980s. Today, only nine rainfall stations that deliver data to WMO standards were reported by their study, which results in a coverage of one rain gauge per 30 000 km<sup>2</sup>. Additional stations are installed, but their data are not freely available and data quality might be heterogeneous.

The number of satellite products covering West Africa increased at the same time. Examples are products from the Global Precipitation Mission (GPM) or Meteosat Second Generation

 Denotes content that is immediately available upon publication as open access.

*Corresponding authors:* Christian Chwala, christian.chwala@kit.edu; François Zougmore, zougmore@ujkz.bf

DOI: 10.1175/JHM-D-23-0015.1

© 2023 American Meteorological Society. This published article is licensed under the terms of a Creative Commons Attribution 4.0 International (CC BY 4.0) License



(MSG) SEVIRI. However, the quality of satellite rainfall estimates suffers due to several reasons. Low-Earth-orbiting (LEO) satellites have a relatively high spatial resolution and sometimes even employ active microwave sensors. But these LEO satellites have long revisit times. Even when using data from a group of LEO satellites, like the GPM constellation (consisting of LEO satellites with passive microwave sensors and one with a dual-frequency radar), the revisit time in the tropics is still approximately 3–4 h (Kidd et al. 2021). Geostationary (GEO) satellites, on the other hand, can provide a subhourly resolution but have to employ highly parameterized retrieval algorithms using only cloud-top observations in the visible and infrared spectra (Rios Gaona et al. 2017; Maggioni et al. 2016; van het Schip et al. 2017). To combine the advantages of LEO and GEO satellite observations, products like IMERG (Huffman et al. 2018) provide a fusion of both types of satellite data. However, IMERG still has shortcomings involving biases (Maranan et al. 2020), and its near-real-time products have a latency of several hours. The lack of ground-based observations for the calibration or validation of satellite products in West Africa is a further issue. Rainfall data from reanalyses improved in the past decade (e.g., from ERA-Interim to ERA5), but large biases persist (Gleixner et al. 2020). Not a single operational weather radar system is deployed in West Africa.

The issue of poor coverage of rainfall can be addressed by the use of opportunistic rainfall information derived from commercial microwave links (CMLs). For more than a decade, rainfall estimation from attenuation of CMLs has been investigated as an alternative to conventional rainfall observations. Early work on CMLs was done in Israel (Messer et al. 2006) and the Netherlands (Leijnse et al. 2007). This was followed by many case studies and method developments, for example, in the Czech Republic (e.g., Fencil et al. 2014), Germany (e.g., Chwala et al. 2012), Sweden (e.g., van de Beek et al. 2020), Israel (e.g., Ostrometzky and Messer 2018), and Italy (e.g., Cazzaniga et al. 2022). Countrywide rainfall estimation was done in the Netherlands (Overeem et al. 2016b), Germany (Blettner et al. 2022; Graf et al. 2020), and Sri Lanka (Overeem et al. 2021).

In Africa, the first results of CML rainfall estimation were successfully obtained in Burkina Faso (Doumounia et al. 2014). The study was conducted in the north-central region of Burkina Faso using a 29-km-long CML with a frequency of 7 GHz. A correlation of 0.8 was achieved with daily rain gauge data. Another study analyzed the pluvial flooding in the city of Ouagadougou in September 2009, using a 7.5-km-long CML with a frequency of 13 GHz (Doumounia et al. 2019). The correlation between hourly data of the CML and a rain gauge was 0.63. More recently, Kumah et al. (2021) used MSG data to derive wet and dry periods along one CML in Kenya. In a follow-up study, they merged data from several CMLs with cloud-top properties measured by MSG satellite data to improve the MSG rainfall estimates with a resolution of 30 min and 3 km  $\times$  3 km (Kumah et al. 2022). Preliminary results for CML-based rainfall estimation in Nigeria including rainfall maps for several hours over the city of Lagos were recently shown in a report by the Groupe Speciale Mobile Association (GSMA) (Pribe and Panos 2023). Other African countries

such as Zambia, Kenya, Niger, and Cameroon are in the proof-of-concept phase for CML data acquisition and rainfall estimation.

CML rainfall data in Europe are on the pathway to being used in operational rainfall products, and many studies discuss the potential of CMLs for African countries. Nevertheless, in Africa, no rainfall maps derived solely from CMLs have been generated and evaluated quantitatively over a longer period, so far. Therefore, the objectives of this study are 1) to derive rainfall maps with high temporal and spatial resolution from a CML network in Ouagadougou, Burkina Faso, for the monsoon season 2020, and 2) to analyze the quality of these rainfall maps in a part of the world where ground-based reference data are sparse.

## 2. Study region and data

The study region is the city of Ouagadougou, the capital of Burkina Faso. The analyzed period is from 14 June to 10 October 2020, which covers almost the complete monsoon season.

### a. Rainfall regime and observational data in Burkina Faso

Located in the heart of West Africa, Burkina Faso has a climate characterized by the succession of two main seasons: the dry season (mid-October to April) and the monsoon season (May to mid-October). The average annual rainfall ranges from 1300 mm in the south (Sudanian zone) to less than 400 mm in the north (Sahelian zone). Rainfall is characterized by strong space–time variability and intermittency (Vischel et al. 2011). Most rain events are short and intense and stem from convective storms. This study focuses on a dense CML network in the city of Ouagadougou located in the center of the country (Sudano–Sahelian zone). The rainfall here is at an intermediate level within Burkina Faso, totaling nearly 800 mm yr<sup>-1</sup> and almost exclusively accumulating during the monsoon season.

### b. CML data

CML data in Burkina Faso were acquired in cooperation with Telecel Faso, a cellular telephone operator in Burkina Faso. A real-time data acquisition (DAQ) system collecting CML data, based on the pySNMPdaq software (Chwala et al. 2016), was set up at the Laboratoire de Matériaux et d'Environnement (LA.ME) of Joseph KI-ZERBO University of Burkina Faso. This real-time DAQ system, described by Djibo et al. (2023b), started as a pilot project covering only eight CMLs and has been progressively expanded. For the 2020 monsoon season, data from more than 1000 CMLs in Burkina Faso with a temporal resolution of 1 min were collected. Often, the CMLs are configured with dual polarization and multifrequencies such that up to eight CMLs are deployed along the same path. Instantaneous measurements of the transmitted signal level (TSL) and received signal level (RSL) were requested every minute from both ends of each CML.

We use data from a dense network of 300 CMLs in the area of Ouagadougou. We chose this area for two reasons. First, only for Ouagadougou, both a dense CML network that can be used to derive rainfall maps and a rain gauge to validate

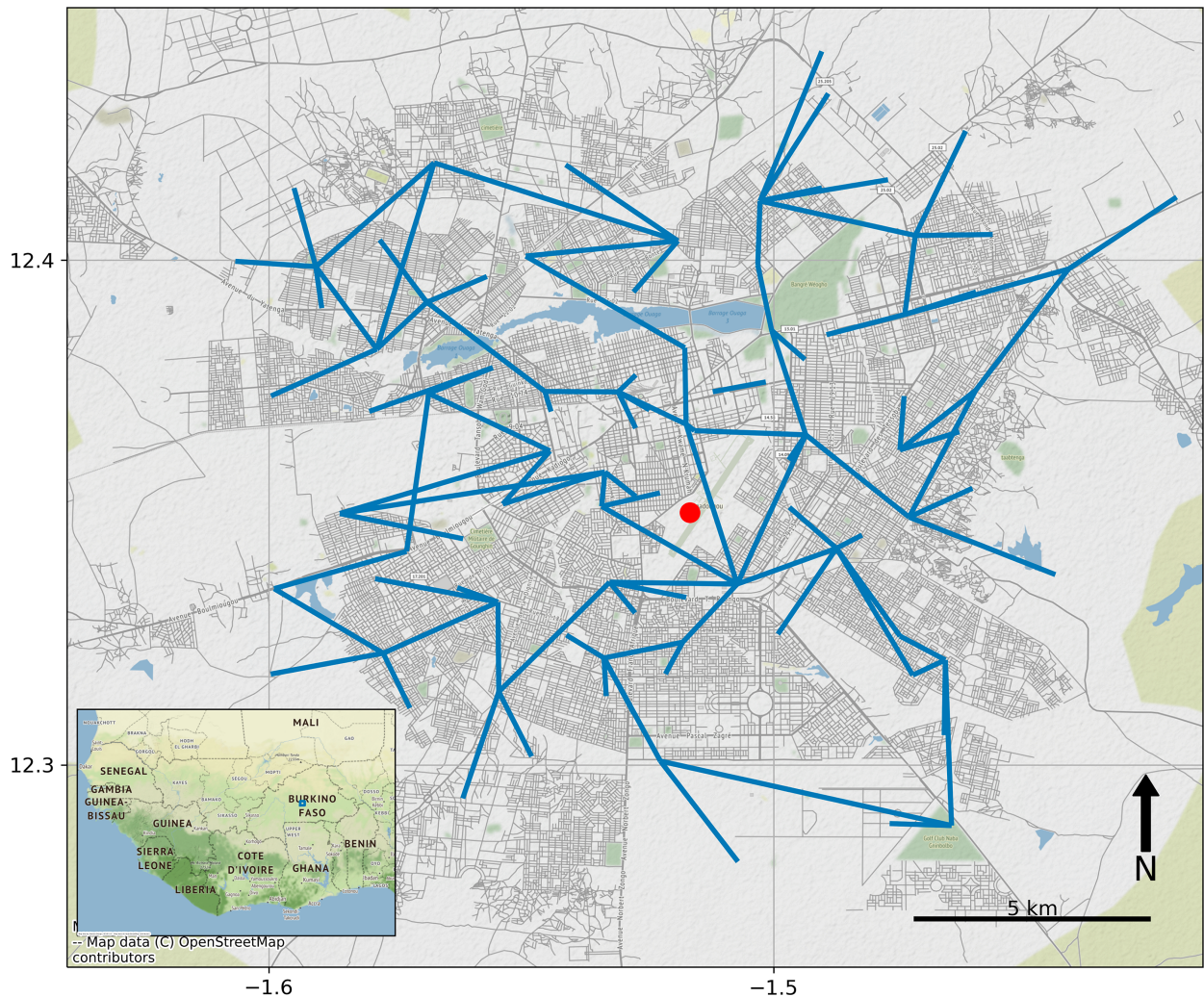


FIG. 1. The topology of the CML network in the region of the city of Ouagadougou showing the sensors used in this work. The red dot indicates the position of the reference rain gauge, and the blue symbol in the inset map indicates the location of the study region in West Africa.

those rainfall maps are currently available for research purposes. Second, most of the CMLs outside of Ouagadougou are long-distance CMLs with a frequency of 7 GHz. Their processing is more challenging due to their lower sensitivity to rainfall and the higher sensitivity to changes in drop-size distribution (see Fig. 3). In addition, interpolated rainfall maps from the currently available CML data cannot produce reasonable results, due to the sparsity of the network [see Fig. 3a in Djibo et al. (2023b)].

The CML data and metadata were transformed from raw CSV files into the netCDF format following the naming conventions and structure of the examples given in the CML processing software package pycomlink (Chwala et al. 2022). The data are stored with equally spaced 1-min time stamps.

The 300 CMLs (mostly consisting of two sublinks) available in Ouagadougou are situated along 119 individual paths, with up to eight CMLs being located on the same path. We excluded 7 CMLs with 7 GHz from the analysis as well as

17 CMLs with less than 50% data availability during the analyzed period and 17 CMLs that derive more than 2 times the amount of rainfall than the average CML (CML rainfall estimation is described in section 3). The latter 17 CMLs did not show distinct similarities in length or frequencies when compared with the rest of the CMLs.

Because the removed CMLs sometimes share a path with one or more other CMLs, 259 CMLs along 100 individual paths remained for the analysis. The CMLs paths are between 0.2 and 7.6 km long with frequencies ranging from 10 to 13 GHz. Figure 1 shows the 100 CML paths used to derive rainfall maps after the filtering and processing of the CMLs, as described in section 3.

### c. Rain gauge data

To validate the rain rates derived from CMLs, we could use only one rain gauge. This gauge was in the city of Ouagadougou, and only data from this single rain gauge, operated by

ANAM, are available for the 2020 monsoon period. This shows, again, the extreme data scarcity of traditional rainfall observations in the region and West Africa in general. The gauge is located at the international airport of Ouagadougou (Fig. 1). The resolution is a daily accumulation from 0600 to 0600 LT, which is manually collected by ANAM agents. Thus, for all quantitative comparisons with rain gauge data, we aggregate the CML-derived rainfall information to daily rainfall sums from 0600 to 0600 of the following day.

#### d. Gridded reference data

In addition to the one rain gauge, we use three gridded precipitation products as references: ERA5, GPM IMERG early run, and GPM IMERG late run. ERA5 is a reanalysis product from ECMWF providing multiple atmospheric variables, including precipitation with a spatial resolution of  $0.25^\circ$  and a temporal resolution of 1 h (Hersbach et al. 2020). IMERG is a multisatellite product available with different latencies. Here, we used the early run with a minimum latency of 4 h and the late run with a minimum latency of 10 h. Both products are from version 06B and have a spatial resolution of  $0.1^\circ$  and a temporal resolution of 0.5 h (Huffman et al. 2018). We derived all three datasets for the whole monsoon period. For validation, we used the pixel closest to the rain gauge from each of the three datasets for a validation against the rain gauge and the CML rainfall map pixel at the same location.

#### e. Disdrometer data

No disdrometer data are available for Ouagadougou. The closest location with available disdrometer observations is Nazinga, Burkina Faso, located 120 km south of Ouagadougou. The data were collected by an OTT Parsivel disdrometer from 1 October 2016 to 26 September 2017 with a temporal resolution of 1 min. We used these observations to validate the International Telecommunication Union (ITU)-recommended attenuation–rainfall rate ( $k$ – $R$ ) relation for 7 and 13 GHz with horizontal and vertical polarization. The calculation of  $k$  from DSD data was carried out using the T-matrix (Mishchenko et al. 1996) method with the software package `pytmatrix` (Leinonen 2014) for a temperature of  $30^\circ\text{C}$ .

### 3. CML data processing

The conversion of CML attenuation data to rainfall rates is challenging since CMLs are an opportunistic data source in the sense that they are not intended for rainfall observation (Uijlenhoet et al. 2018). Thus, the processing of CML data has a large impact on the quality of the generated rainfall information and must be done carefully. Most CML research groups have developed their own methods tailored to their needs and datasets. An overview of these methods is given by Chwala and Kunstmann (2019). For our analysis, we use the methods available in the Python package for CML processing, `pycomlink`. We follow the processing chain developed for the countrywide CML rainfall estimation in Germany (Graf et al. 2020), adapt it to our dataset, and extend it with new filtering of CML data anomalies. In the following sections, we describe

the resulting processing chain. The lettering of the sections follows the order of the processing steps.

#### a. Data preparation

The CML data contain invalid records from missing time steps due to data acquisition failures, missing values [i.e., not a number (NaN)], and default fill values (e.g.,  $-99.9$  in RSL or  $250.0$  in TSL), which we set to NaN. To increase data availability, we linearly interpolated gaps of up to 10 min in the raw total loss (TL; difference between TSL and RSL). For example, such gaps can be a result of short outages of the data acquisition system. For each CML, we neglected data from additional sublinks and used the first sublink that was listed in the database to derive rainfall estimates with the following processing steps.

#### b. Filtering CML data

Besides invalid records, the CML data can include anomalies such as steps (sudden change in the baseline of a CML) and spikes (strong positive outlier at individual time steps) that are within the dynamic range of signal levels but have to be filtered because they can create considerable amounts of false-positive rainfall. The reasons for such erratic behavior are not understood but are known to include multipath propagation, for example, above-water bodies, which are shown in Fig. 1; swinging masts; or the influence of radiation and temperature on the CML equipment, as well as moving objects in the line of sight of CMLs. To account for such issues, we developed three filters for the specific needs of the CML data in Burkina Faso, which are replacing the filtering of Graf et al. (2020). We applied a filter to detect and remove steps, a filter to detect and remove spikes, and a filter to detect and remove periods with too many short NaN gaps.

To detect steps, we first applied a centered 3-day rolling median of TL. If TL jumps to a new baseline (see section 3d), this rolling median changes. To quantify this change, we calculated the absolute difference between the centered 4-h rolling maximum and minimum of this 3-day rolling median and removed time steps as steps when this difference was larger than 1 dB. This filter removed 0.035% of all data points.

To detect spikes, we compared each TL value with both its immediately preceding and subsequent time steps. If both the preceding and the subsequent time steps were 5 dB smaller than the current time step, we classified it as a spike and removed the value. This filter removed 0.042% of all data points.

Periods with too many NaN values occurring frequently as short gaps might be problematic due to the interpolation of gaps up to a length of 10 min that we apply (see section 3a). For a time series with many short gaps, this potentially results in a large number of interpolated data points. Therefore, we removed all periods where at least 50% of the data are missing completely. Within the dataset, these gaps were often short ( $<1$  h) but frequent. This filter removed 0.100% of the data.

By only excluding time steps and periods that are affected by steps, spikes, or periods with many missing data points, we were able to preserve data in comparison with the previous

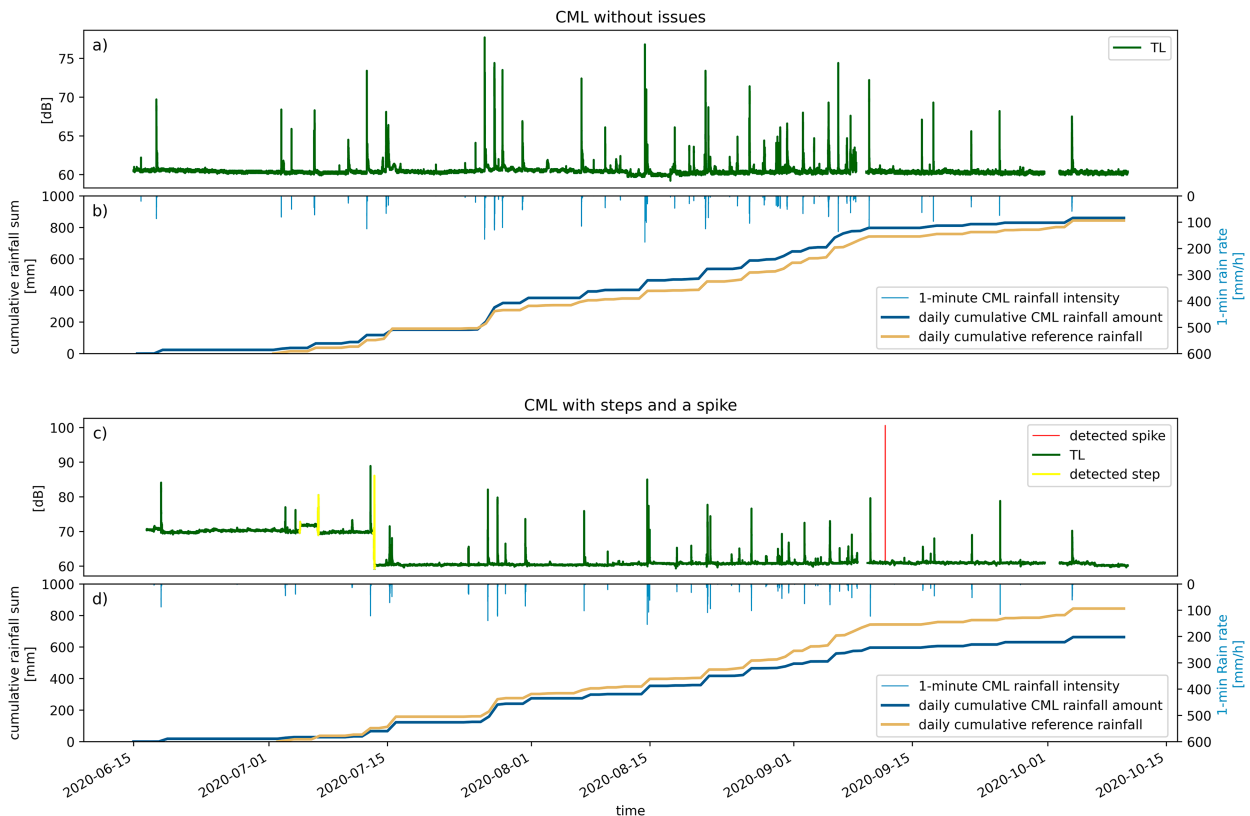


FIG. 2. Comparison of CML rainfall time series with daily rain gauge data. (a) The CML without issues has a frequency of 13.17 GHz and a length of 1.68 km. (c) The CML with steps and spikes has a frequency of 10.84 GHz and a length of 3.70 km. The TL time series (dB) in (a) and (c) have a 1-min resolution. (b),(d) The rain rate  $R$  ( $\text{mm h}^{-1}$ ) has a 1-min time resolution and is complemented by a comparison of cumulative rainfall sum (mm) between the reference and CML.

filtering methods of Graf et al. (2020), which excluded suspicious CMLs on a monthly basis. To improve data availability, we repeated the interpolation of TL gaps of up to 10 min to close gaps caused by the step and spike filter. After filtering and interpolating TL, a total of 0.132% of data were removed from the analysis. Figure 2 shows data from two types of CML that illustrate the filtering: the first CML has a TL that is not affected by steps or spikes, while the TL of the second one is affected. The affected CML was corrected by the filters as described above and showed good results after filtering.

### c. Rain event detection

The separation of wet and dry periods is crucial as errors made in this step will impact the performance of the rainfall estimates: missed rain events will lead to an underestimation of precipitation, and the false detection of rain events will lead to an overestimation (Polz et al. 2020). The task of detecting rain events in the TL time series is straightforward for strong rain events. The detection becomes more and more difficult when the rain-induced attenuation approaches the same order of magnitude as the signal fluctuations during dry conditions. Two different concepts for wet–dry classification have been proposed: one compares the TL of a certain CML with

that of neighboring CMLs (Overeem et al. 2016a), and the other studies the time series of each CML separately (Chwala et al. 2012; Ouedraogo et al. 2022; Polz et al. 2020; Schleiss et al. 2013; Wang et al. 2012). The first method was developed for 15-min minimum–maximum TL data. The later methods have been developed for TL data with higher temporal resolution.

We apply the wet–dry classification method proposed by Schleiss and Berne (2010), which uses a rolling standard deviation of the TL with an individual threshold for each CML. We set the threshold to the 85% quantile of the 60-min rolling standard deviation multiplied by a factor 1.2. The threshold and factor are slightly higher (5% for the quantile and 0.08 for the factor) than the ones we used from Graf et al. (2020). The threshold and factor were not optimized with reference data but were slightly adjusted based on experience and the rainfall regime in Burkina Faso, which is typically intense and of short duration as compared with the moderate rainfall in Germany. Hence, we do not face the challenge of detecting long-lasting, low-intensity rain events, which are hard to distinguish from TL fluctuations during dry periods. Using higher thresholds decreased the chance of producing false-positive results.

#### d. Baseline and wet antenna attenuation

The path-integrated attenuation due to rainfall can be retrieved from TL by subtracting the baseline attenuation during dry conditions and the additional attenuation due to antenna wetting (WAA) (Schleiss et al. 2013; Zinevich et al. 2010). The baseline was assumed to be equal to TL at the time step before a rain event and to remain constant during the event. WAA is estimated following the time-dependent approach of Schleiss et al. (2013), which was preferred over the rain-rate-dependent method of Leijnse et al. (2008), which we used in previous studies. This is based on two facts: First, the approach from Schleiss et al. (2013) should not suffer from the issue of underestimation of very small rainfall intensities, which we found in Germany, since rainfall events in Burkina Faso are intense and short. Second, with such high-intensity events and no upper limit for WAA in the rain-rate-dependent approach of Leijnse et al. (2008), there could be an overestimation of WAA.

The maximum WAA value was set to 2.5 dB, which is slightly larger than the 2.3 dB proposed by Schleiss et al. (2013), and  $\tau$ , which controls the speed of approaching the maximum WAA, was set to 15 min, as proposed by these authors. However, the magnitude of WAA is still a subject of uncertainty that cannot be completely resolved even with dense reference data (e.g., Pastorek et al. 2022).

#### e. Calculation of rain rate from attenuation

The technique for deriving rain rates from attenuation is based on the close-to-linear relationship between specific attenuation  $k$  (dB km<sup>-1</sup>) and rain rate  $R$  (mm h<sup>-1</sup>) (Atlas and Ulbrich 1977), given by

$$k = aR^b. \quad (1)$$

In this equation,  $a$  and  $b$  are constants that depend on frequency, and polarization (horizontal or vertical). Note that the  $k$ - $R$  relation is fairly insensitive (as compared with the radar  $Z$ - $R$  relation) to DSD variations for frequencies ranging between 15 and 35 GHz. The rain rates derived from the CML attenuation data are provided with a temporal resolution of 1 min. Figure 3 shows the relationship between rain rates  $R$  derived from disdrometer data from Nazinga and the specific attenuation  $k$  derived using values for  $a$  and  $b$  from the ITU-Radiocommunication Sector (ITU-R) (ITU-R 2005) for 7 and 13 GHz. As expected, for 7 GHz, the relation is subject to larger errors. To derive rain rates from the CML attenuation values via the  $k$ - $R$  relation, we used  $a$  and  $b$  values from ITU-R (2005).

#### f. Rainfall maps

In case more than one CML along the same path was available, we selected the one with the rainfall sum closest to the average rainfall sum to all CMLs. We accounted for the temporal availability of a CML by aggregating all other CMLs only over those periods when the compared CML was available.

We used the same inverse distance weighting (IDW) approach used in Graf et al. (2020) for hourly CML rainfall estimates in Germany to interpolate the CML data in Burkina Faso on a 5-min basis. We chose this method over options like ordinary kriging because Graf et al. (2020) found only marginal gains when using kriging with fixed or monthly adjusted semivariogram parameters relative to IDW. In addition, the 1-h rainfall maps from the German study can be assumed to introduce less uncertainty to the variogram estimation step than the 5-min resolution in this study would. Also, IDW needs comparatively little computational effort.

Each CML rainfall value is represented by a synthetic point observation at the center of the CML path (e.g., as done by Overeem et al. 2013). Eshel et al. (2021) only found marginal improvements when iteratively using several points along the CML paths for CMLs with an average length of 7.64 km. We assume that for the CMLs in Ouagadougou with an even smaller average length of 2.21 km, such improvements are negligible. For each pixel of the interpolated rainfall field, the 16 closest CML observations at the center point of the CML are taken into account and the weights decrease with the distance  $d^2$  (km). The average distance to the next closest center point from each CML's center point is 0.89 km. The resulting rainfall maps have a spatial resolution of 0.55 km. The rainfall maps were published with an example animation (Djibo et al. 2023a).

#### g. Evaluation metrics

In this section, we describe the performance measures that are used for validating the CML-derived rainfall information data against the reference data.

We use the Pearson correlation coefficient (PCC) to measure the degree of linear correlation between the CML-derived rainfall and the reference. It is given by

$$\text{PCC} = \frac{\text{Cov}(R_{\text{CML}}, R_{\text{reference}})}{\text{SD}(R_{\text{CML}})\text{SD}(R_{\text{reference}})}, \quad (2)$$

where  $R_{\text{reference}}$  is the daily rain rate from the rain gauge and  $R_{\text{CML}}$  is the daily aggregation of the CML-derived, 5-min rainfall maps at the location of the reference rain gauge. The covariance function is denoted by Cov, and SD is the standard deviation function.

The coefficient of variation (CV) shows the variability of the error of CML rainfall estimates relative to the reference. It is given by the ratio of the residual standard deviation (SD) to the mean rainfall at the reference. The higher the value of the coefficient of variation is, the greater is the dispersion around the mean. The coefficient of variation can be written as

$$\text{CV} = \frac{\text{SD}(R_{\text{CML}} - R_{\text{reference}})}{\bar{R}_{\text{reference}}}. \quad (3)$$

In addition, we calculated the mean absolute error (MAE; mm) and root-mean-square error (RMSE; mm) to measure the accuracy of the CML rainfall estimates. MAE and RMSE are respectively defined as

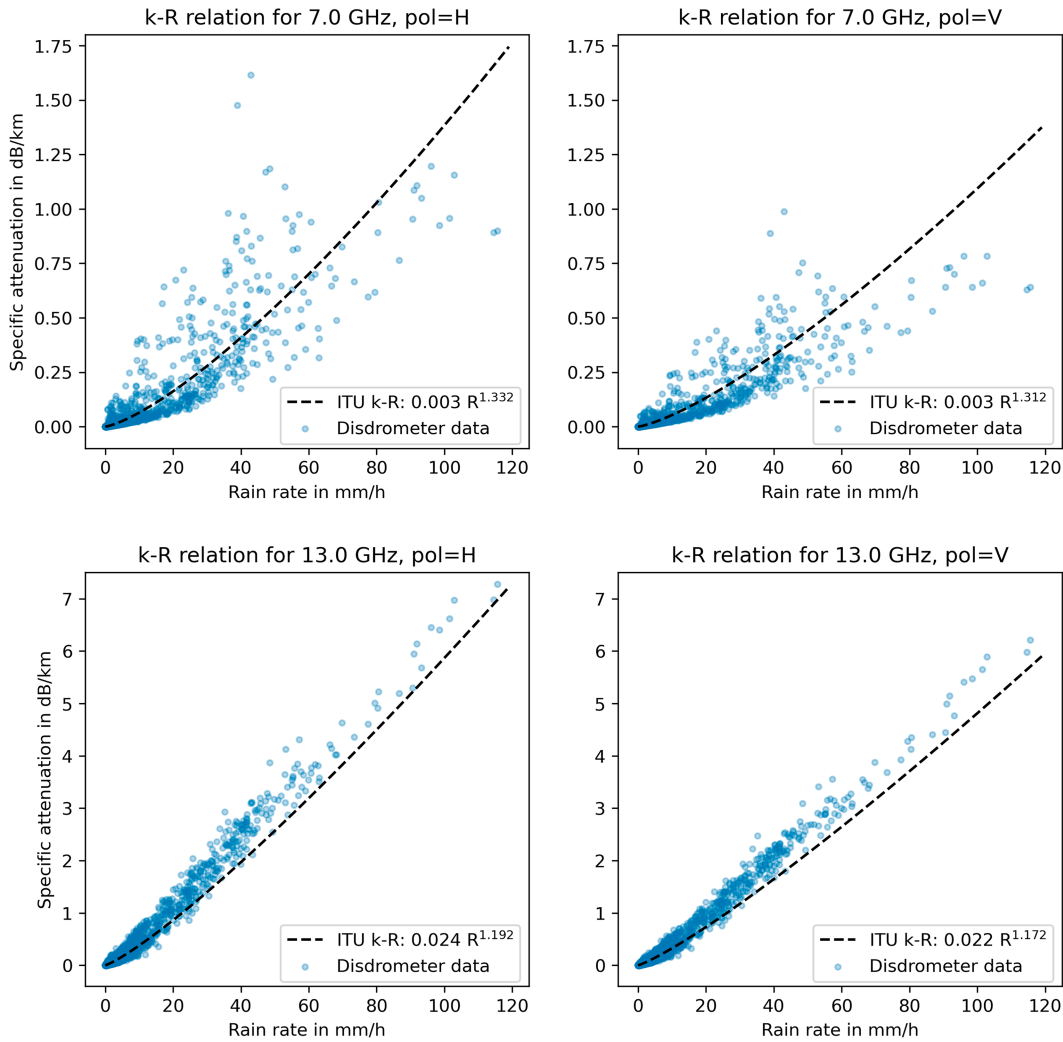


FIG. 3. Comparison of  $k$ - $R$  relation obtained with DSD data from an OTT Parsivel disdrometer at Nazinga (blue dots), and the  $k$ - $R$  relation of the ITU (black dashed line) for 7 and 13 GHz with horizontal and vertical polarization.

$$MAE = |R_{CML} - R_{reference}| \quad \text{and} \quad (4)$$

$$RMSE = \sqrt{(R_{CML} - R_{reference})^2}. \quad (5)$$

The relative bias measures the average deviation between the reference and the CML rain rate relative to the average reference rainfall. It is given by

$$bias = \frac{(R_{CML} - R_{reference})}{R_{reference}}. \quad (6)$$

#### 4. Results and discussion

The goal of this study is to produce CML rainfall maps with a high spatial and temporal resolution. To verify their added information content, we analyze their spatial and temporal

representativeness. Since the reference rain gauge data are sparse and at a coarse daily resolution, we follow two different strategies to evaluate the CML rainfall estimates against the rain gauge. First, we perform a qualitative analysis of the CML-derived rainfall maps and check their spatial and temporal consistency in sections 4a–c. Second, we evaluate the interpolated rainfall maps at the location of the rain gauge. In this approach, we had to compare daily rainfall aggregates with the reference due to the limited temporal resolution of the reference. Additionally, we use three gridded datasets from satellites and reanalyses with a higher temporal resolution to compare them with the rainfall estimates from the rain gauge and CML rainfall maps.

##### a. Qualitative analysis of 5-min rainfall maps

In Sahelian West Africa, rain events are typically short and intensive, with an average duration of 1 h (Moumouni et al. 2008). Only rainfall maps with high temporal resolution, well

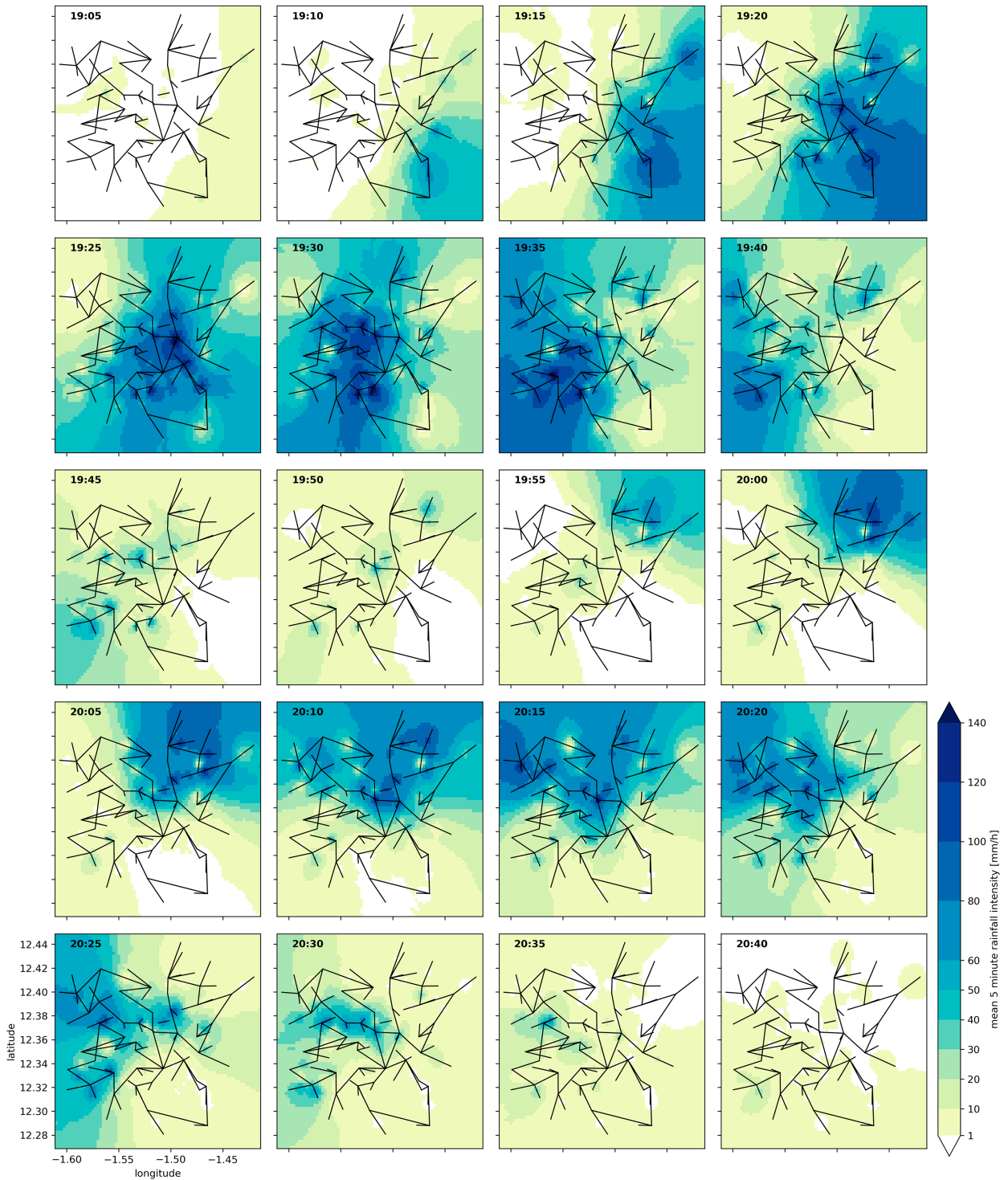


FIG. 4. Example of CML-derived, 5-min rainfall maps for the city of Ouagadougou. The black lines indicate the CML paths. An animation of these rainfall maps is available in [Djibo et al. \(2023a\)](#).

below the daily scale, can reveal the spatiotemporal dynamics of these events. Because of the limited reference data, we performed a qualitative analysis of the rainfall maps interpolated from 5-min CML rainfall sums. For visual inspection, we chose

a rain event on 21 August 2020. It started at 1905 UTC and ended at 2045 UTC. As displayed in [Fig. 4](#), the CML-derived rainfall maps show a reasonable spatiotemporal evolution of the rainfall field. An animation of the shown 5-min rainfall



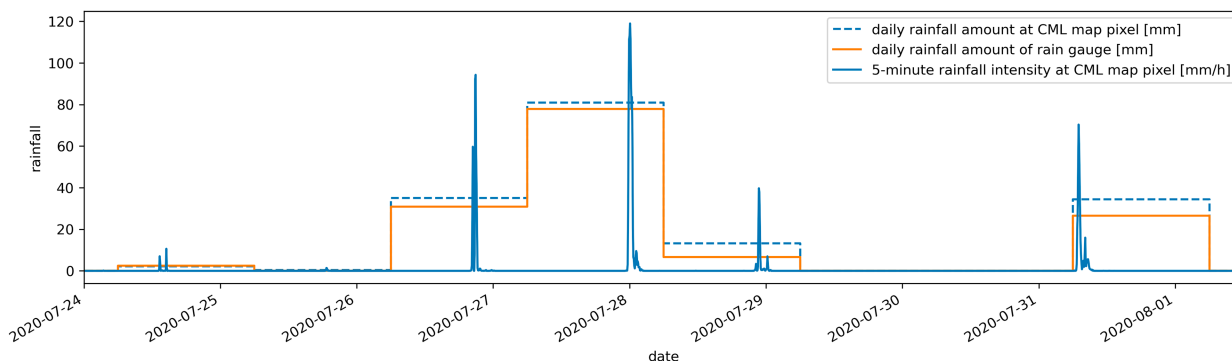


FIG. 5. Time series of rain gauge data and of the rainfall map pixel at the rain gauge location. The daily rainfall amount from CMLs and the daily rainfall amount of the rain gauge are given in millimeters per day, and the 5-min rainfall intensity from CMLs is given in millimeters per hour.

maps was published together with the actual data of the rainfall maps for the monsoon season 2020 (Djibo et al. 2023a). Within the event, one can see two distinct rain cells moving over the city of Ouagadougou from east to west. Even though, at the center points of individual CMLs, considerable higher or lower values are visible in the rainfall maps as a result of the IDW interpolation, the high density of CML observations in the domain reveals local structures and the limited spatial extent of the rainfall event. Hydrological applications like flood forecasting can profit from such rainfall maps as rain gauges are usually far apart in this region of the world.

#### b. Visual validation of 5-min rainfall maps at location of daily rain gauge

A comparison between the cumulative rainfall sums derived from individual CMLs and the reference rain gauge over the entire 2020 monsoon period shows good agreement (see Fig. 2). To illustrate the performance of the interpolated rainfall maps, we show a validation of the 5-min precipitation maps at the pixel of the daily rain gauge. Figure 5 shows five distinct rainfall events in 1 week from the daily rain gauge ( $\text{mm day}^{-1}$ ) and the 5-min precipitation maps ( $\text{mm h}^{-1}$ ) and their daily aggregation (mm). For the first three events, the CMLs match the reference well while also providing a high-resolution timing of the rain events. The last two rain events show an overestimation of the CMLs with respect to the reference. This can potentially be explained by a spatial gradient of rainfall close to the rain gauge or by unknown factors influencing the CML rainfall estimation (e.g., slow drying of wet antenna due to clouds or low wind; different DSD).

#### c. Qualitative analysis of daily rainfall maps

For a qualitative comparison with the reference, we aggregate the 5-min CML-derived rainfall maps over the aggregation interval of the rain gauge data, that is, daily from 0600 to 0600 the day after. This allows us to see the spatial distribution of the rainfall events and to check how good the rainfall fields fit to the point observation of the gauge in the center of our domain. Figure 6 shows the daily aggregations of the 5-min rainfall maps from 29 June 2020 to 10 October 2020 and depicts the position of the reference rain gauge (red circle)

and its rainfall sum (color within the red circle). The period of 14–28 June 2020 was a very dry period and, therefore, omitted. In general, the CML rainfall maps are in very good agreement with the reference, with a PCC of 0.97 and an RMSE of 4.06 (see performance metrics for 0-km radius in Fig. 8, described in more detail below).

While some CMLs may show an under- or overestimation of rainfall relative to the reference data, the CML network provides unique rainfall information in this area. The two main achievements are the spatial representativeness of the rainfall maps for the whole city and the high temporal resolution of 5 min.

#### d. Validation of daily rainfall maps generated from synthetically thinned-out CML networks

Since the values of the interpolated rainfall maps at the gauge location are dominated by the CMLs close to the rain gauge, we conducted an additional validation of the CML-derived rainfall maps whereby we removed the CML paths that have their center point within a circle around the gauge with three different radii (1, 3, and 5 km). For each synthetically thinned-out CML network we generated a new set of 5-min rainfall maps that were then aggregated to daily maps. Figure 7 shows the original and thinned-out CML networks.

#### e. Quantitative analysis of daily rainfall sums

We calculated all performance metrics between daily aggregates of the interpolated 5-min rainfall maps at the reference location and the reference rain gauge using the full study period. Each metric is calculated for each of the CML networks discussed in the previous section and depicted in Fig. 8. All metrics (except for the relative bias) show little difference for the 0-, 1-, and 3-km radii, whereas the 5-km radius results in worse metrics. Only the bias shows differences, with the lowest bias achieved at a 1-km radius. Overall, the metrics show a high agreement between the reference and the different subset of CMLs even for the 5-km radius. These results suggest not only that the CMLs close to the reference rain gauge but also the ones at greater distances deliver trustworthy rainfall estimates. This emphasizes the spatial representativeness of individual CMLs and, in turn, the robustness of the derived

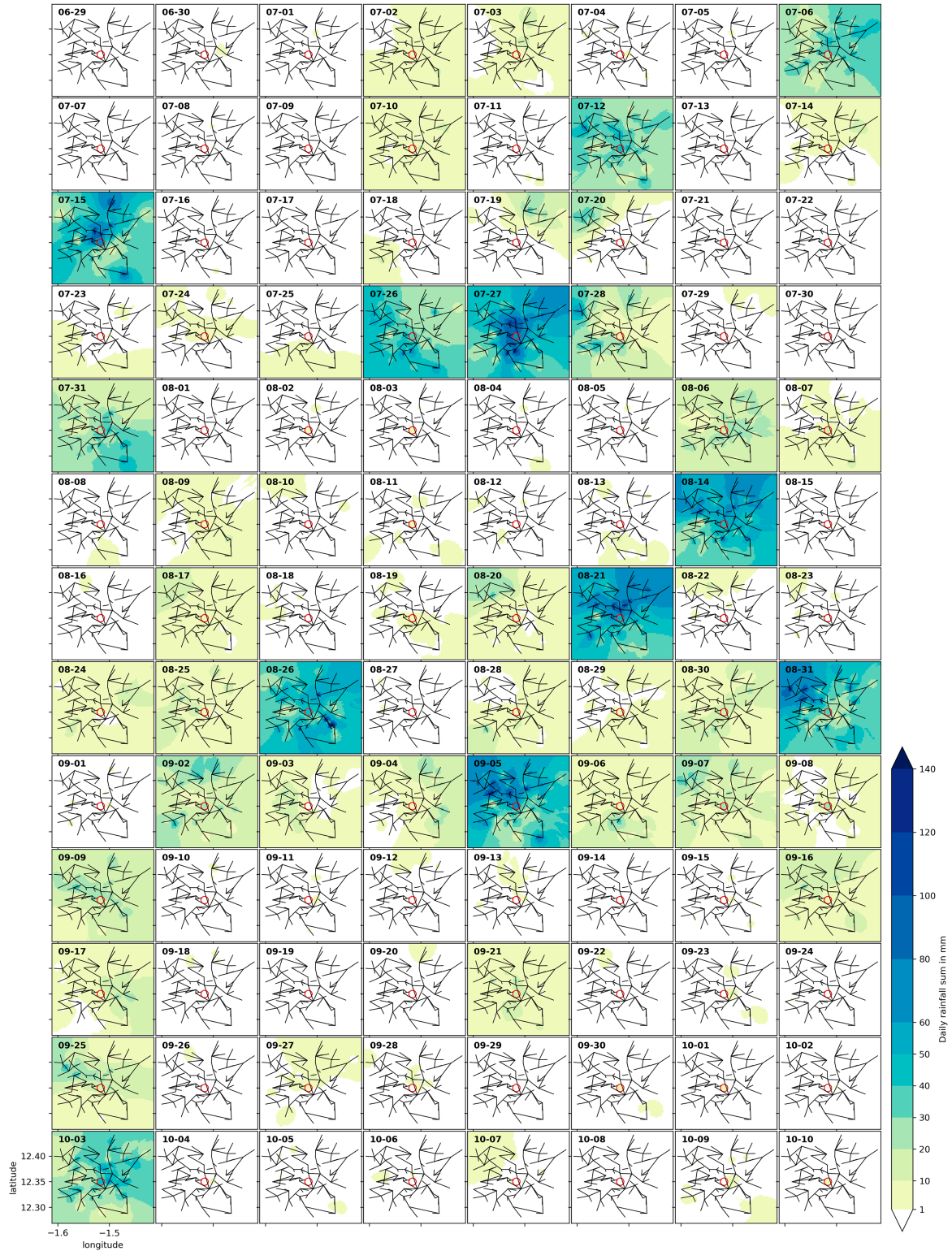


FIG. 6. Daily CML-derived rainfall maps aggregated from the 5-min maps. Daily rain gauge data are shown with the same color scale for comparison. The red open circle indicates the position of the rain gauge.

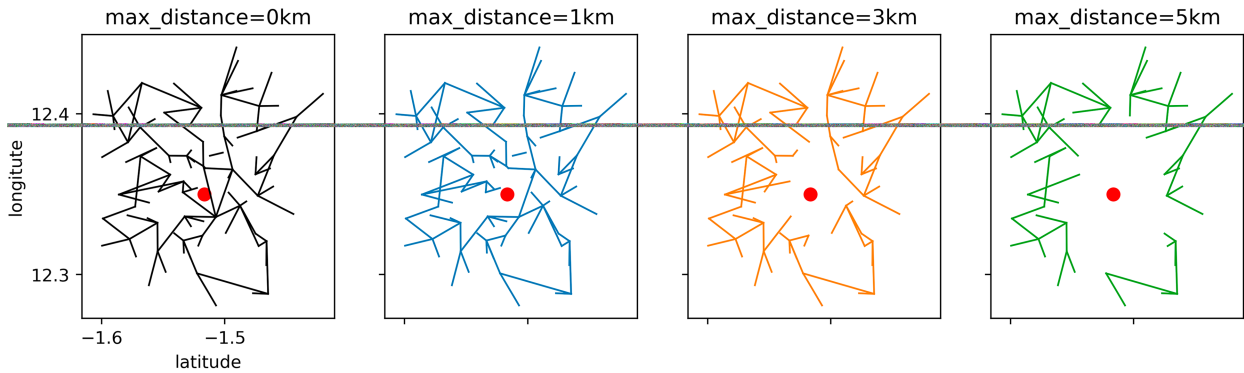


FIG. 7. (left) Maps of the original and the synthetically thinned-out CML network. The red dot indicates the position of the rain gauge.

daily rainfall maps even in areas of lower CML network density. By collecting more CML data from several monsoon seasons, this evaluation could be used to quantify the spatial decorrelation length of rainfall in Ouagadougou using a similar approach as presented by Eshel et al. (2022).

*f. Comparison with the performance of other gridded precipitation products*

Since the validation with the rain gauge is limited to a daily resolution and a single location, we used three gridded precipitation products with a temporal resolution of 0.5 and 1 h. First, we compared the daily aggregations from these three products and the CML maps with the reference rain gauge in Fig. 9. ERA5, which is the product with the coarsest spatial resolution, showed the worst performance, especially for medium to high daily rainfall sums. The early and late run of GPM IMERG compared better to the reference, albeit high daily rainfall sums underestimated by the early run and the late run showed a large scatter for high daily rainfall sums. The CML rainfall map showed the least error at the location of the rain gauge from all products. Therefore, we conclude that the daily rainfall sum of all three gridded reference products cannot be used directly for a quantitative evaluation of the CML rainfall maps. However, the spatial precision of the CML rainfall maps can be assumed to be higher than the precision of the gridded reference products when compared with the point observation of the rain gauge.

When looking at the temporal coincidence of rain events between the CML rainfall maps aggregated to a 30-min resolution and the IMERG early run, we found a high agreement. It is reasonable to assume that the temporal localization of rain events in IMERG early run is precise. However, the rainfall amount differs quite strongly between CMLs and IMERG, with higher and shorter peaks in the CML rainfall map. This was expected from the daily comparison of rainfall sums, and the broader peaks can be a result of the larger integration volume from IMERG than from the CML rainfall estimates. We chose the IMERG early run for the in-depth comparison because it has the lowest latency and had results similar to the late run when compared with the reference rain gauge. We also did not consider ERA5, as it had the worst performance of all three gridded reference products. In summary, the comparison of daily rainfall sums from the CML rainfall maps and three reference products showed that CML estimates can observe rainfall with a higher precision than re-analysis and satellite products, which had large biases. Also, the high temporal coincidence of the rain events between CML rainfall maps and the IMERG early run supports the correctness of CML rainfall estimates on a subhourly time scale.

**5. Conclusions**

The objective of this study was to produce high-resolution rainfall maps from CML data in Ouagadougou, Burkina Faso, West Africa. We processed 300 CMLs situated along 119 unique

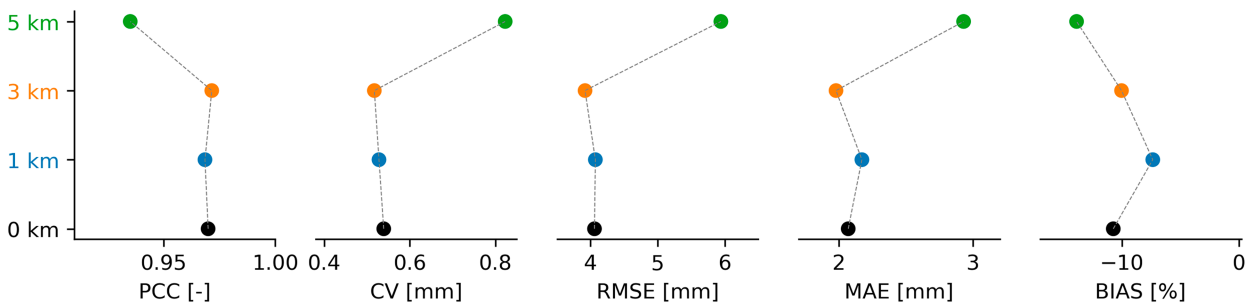


FIG. 8. The results of the rainfall performance metrics for the full and the synthetically thinned-out CML network. Metrics were calculated based on daily values for the whole analysis period.

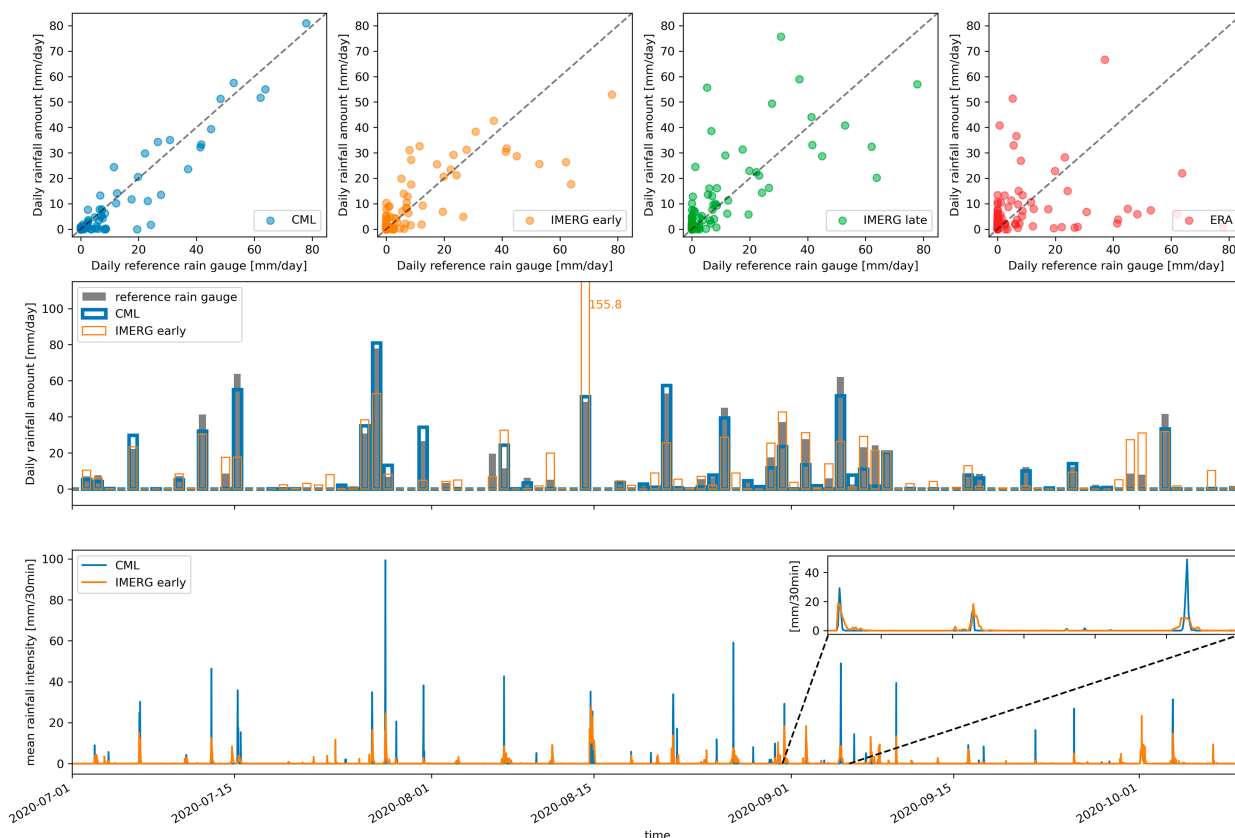


FIG. 9. Comparison of rainfall estimates from CML-derived rainfall maps, GPM IMERG early and late runs, and ERA5 against the daily reference rain gauge from 1 Jul to 10 Oct 2020: (top) Individual scatterplots of all four products at the reference against rain gauge values. (middle) The time series of the CML rainfall maps and the IMERG early run against the reference rain gauge in a daily resolution. (bottom) CML rainfall maps and the IMERG early run on a 30-min resolution; the inset is a zoom over 6.75 days from 0600 UTC 31 Aug to 0000 UTC 6 Sep.

paths in Ouagadougou, using existing processing routines and newly developed filters. After selecting and processing suitable CMLs, we were able to derive rainfall maps based on rainfall information along 100 unique paths. The rainfall maps from CMLs showed promising results for the 2020 monsoon season when compared with the one available reference rain gauge in Ouagadougou.

During processing, spikes and steps, even if not occurring frequently in the TL time series, proved to be an issue causing overestimation of rainfall. Therefore, we developed new filters that remove individual time steps from spikes and steps in order to keep as many of the individual CMLs time series as possible. This increased the data availability relative to methods that removed CMLs with certain anomalies completely. In addition, periods with many short NaN gaps were removed. Another crucial, but well known, step in the processing was the detection of rainfall events in the TL time series. We used the approach proposed by Graf et al. (2020) but set the threshold to a more conservative value because, in comparison with Germany, rain events in Ouagadougou tend to be short and strong, which makes them easier to detect in the TL time series. To compensate for WAA, we used the method of Schleiss et al. (2013), with a

maximum WAA value of 2.5 dB. This, of course, might have an impact on the bias of the rainfall estimates relative to the reference.

The validation of the rainfall maps derived with a simple IDW interpolation scheme against ground-based rainfall data was not straightforward, because only one rain gauge operated by ANAM was available in the whole area of Ouagadougou. Such a situation of sparse reference data is common in West Africa. The rain gauge is, by far, not representative for the whole area of Ouagadougou; therefore, we used various qualitative and quantitative approaches to evaluate the accuracy and show the benefit of CML rainfall estimates.

Visual qualitative analysis of 5-min rainfall maps showed plausible spatial and temporal patterns of rainfall. The comparisons of daily, aggregated, 5-min rainfall maps with the daily reference rain gauge showed good agreement for the temporal distribution of rainfall during the monsoon season as well as a good agreement of daily rainfall sums.

When quantitatively assessing the accuracy of the CML rainfall maps, this agreement was further supported. Even with no CML directly above the rain gauge, the PCC of the reference rain gauge and the corresponding rainfall map pixel was very high. Other metrics proved to be similarly good. We

further investigated whether these metrics were only good due to the good performance of a few CMLs close to the reference rain gauge. We did this by removing CMLs around the rain gauge for several radii before doing the interpolation of the 5-min rainfall maps. When removing CMLs up to a distance of 3 km, no decrease in performance of the rainfall maps relative to the rain gauge was observed. This proved that the performance of the CML rainfall maps on the daily scale was not based on the good performance of one or a few CMLs close to the rain gauge but that the performance is due to the similar high quality of CML rainfall estimates throughout Ouagadougou.

To complement the validation against the daily rain gauge with a higher temporal resolution, we also analyzed three gridded rainfall products (ERA5, IMERG early and late runs). The three products could not match the rainfall amount reference rain gauge as well as the CML rainfall map and, therefore, were not suitable for a validation of CML rainfall estimates. But a surprisingly high temporal coincidence of rainfall events was found between IMERG early (and late) and the CML rainfall maps. This temporal match on a 30-min basis increased the confidence in the CML rainfall maps.

In summary, we provided the first rainfall maps with a 5-min resolution in West Africa based on CML data. Such rainfall maps give an unprecedented option to study spatio-temporal rainfall characteristics and can serve as input for a variety of hydrometeorological applications from flood warning systems to water distribution tasks. The validation of rainfall estimates was and will be challenging in this data-scarce region of the world. One potential way of solving this issue could be the indirect validation of rainfall estimates via hydrological modeling, for example, by building on the hydrological simulations from [Turko et al. \(2021\)](#), who used synthetic simulated CML observations for the region of Ouagadougou. Another major challenge is the processing of 7-GHz CMLs, which are common for the longer connections outside of the cities in West Africa. One way to improve the quality of these CMLs could be the use of satellite data, for example, from MSG SEVIRI. Such a combination could also further improve the high-resolution rainfall maps presented for the city of Ouagadougou.

*Acknowledgments.* We thank Telecel Faso SA, the Top-Raincell project, and the LA.ME laboratory of Joseph KI-ZERBO University of Ouagadougou, Burkina Faso, for the provision of CML data. Top-Raincell has been funded by Fonds National de la Recherche et de l'Innovation pour le Développement (FONRID), the Ministry of Research and Innovation of Burkina Faso, during the 2019–21 monsoon seasons. We further thank ANAM of Burkina Faso for providing the reference data, and WASCAL for making the Nazinga disdrometer data available. This work was supported by the German Ministry of Education and Research (BMBF) via funding for the project AgRAIN (Grant 01LZ1904B).

*Data availability statement.* The CML data supporting this research were provided by Telecel Faso SA within the

Top-Raincell project. These data are not publicly available because Telecel Faso SA restricted the distribution of these data because of their commercial interest. To obtain CML data for research purposes, a separate and individual agreement with the network provider has to be established. The rain gauge data were provided by ANAM and are available upon request. ERA5 data can be obtained, for example, from the Copernicus Climate Data Store (<https://cds.climate.copernicus.eu/>). GPM IMERG data can be obtained from NASA's Goddard Earth Sciences Data and Information Services Center (<https://gpm.nasa.gov/data/directory>).

## REFERENCES

- Atlas, D., and C. W. Ulbrich, 1977: Path- and area-integrated rainfall measurement by microwave attenuation in the 1–3 cm band. *J. Appl. Meteor.*, **16**, 1322–1331, [https://doi.org/10.1175/1520-0450\(1977\)016<1322:PAAIRM>2.0.CO;2](https://doi.org/10.1175/1520-0450(1977)016<1322:PAAIRM>2.0.CO;2).
- Blettner, N., C. Chwala, B. Haese, S. Hörning, and H. Kunstmann, 2022: Combining commercial microwave link and rain gauge observations to estimate countrywide precipitation: A stochastic reconstruction and pattern analysis approach. *Water Resour. Res.*, **58**, e2022WR032563, <https://doi.org/10.1029/2022WR032563>.
- Bliefernicht, J., S. Salack, M. Waongo, T. Annor, P. Laux, and H. Kunstmann, 2021: Towards a historical precipitation database for West Africa: Overview, quality control and harmonization. *Int. J. Climatol.*, **42**, 4001–4023, <https://doi.org/10.1002/joc.7467>.
- Cazzaniga, G., C. De Michele, M. D'Amico, C. Deidda, A. Ghezzi, and R. Nebuloni, 2022: Hydrological response of a peri-urban catchment exploiting conventional and unconventional rainfall observations: The case study of Lambro Catchment. *Hydrol. Earth Syst. Sci.*, **26**, 2093–2111, <https://doi.org/10.5194/hess-26-2093-2022>.
- Chwala, C., and H. Kunstmann, 2019: Commercial microwave link networks for rainfall observation: Assessment of the current status and future challenges. *Wiley Interdiscip. Rev.: Water*, **6**, e1337, <https://doi.org/10.1002/wat2.1337>.
- , and Coauthors, 2012: Precipitation observation using microwave backhaul links in the alpine and pre-alpine region of Southern Germany. *Hydrol. Earth Syst. Sci.*, **16**, 2647–2661, <https://doi.org/10.5194/hess-16-2647-2012>.
- , F. Keis, and H. Kunstmann, 2016: Real-time data acquisition of commercial microwave link networks for hydrometeorological applications. *Atmos. Meas. Tech.*, **9**, 991–999, <https://doi.org/10.5194/amt-9-991-2016>.
- , M. Graf, D. Serebenik, F. Keis, N. Blettner, and Y. Boose, 2022: pycomlink/pycomlink: v0.2.6. Zenodo, <https://doi.org/10.5281/zenodo.4621635>.
- Djibo, M., C. Chwala, M. Graf, J. Polz, H. Kunstmann, and F. Zougmore, 2023a: Rainfall maps from commercial microwave link data for Ouagadougou, Burkina Faso. Zenodo, accessed 13 June 2023, <https://doi.org/10.5281/zenodo.8032918>.
- , and Coauthors, 2023b: Towards innovative solutions for monitoring precipitation in poorly instrumented regions: Real-time system for collecting power levels of microwave links of mobile phone operators for rainfall quantification in Burkina Faso. *Appl. Syst. Innovation*, **6**, 4, <https://doi.org/10.3390/asi6010004>.

- Doumounia, A., M. Gosset, F. Cazenave, M. Kacou, and F. Zougmore, 2014: Rainfall monitoring based on microwave links from cellular telecommunication networks: First results from a West African test bed. *Geophys. Res. Lett.*, **41**, 6016–6022, <https://doi.org/10.1002/2014GL060724>.
- , M. Sawadogo, S. R. Sanou, and F. Zougmore, 2019: Rainfall estimation using commercial microwave links (CMLs) attenuations: Analyse of extreme event of 1st September 2009 in Ouagadougou. *Amer. J. Environ. Prot.*, **8** (1), 1–4, <https://doi.org/10.11648/j.ajep.20190801.11>.
- Eshel, A., H. Messer, H. Kunstmann, P. Alpert, and C. Chwala, 2021: Quantitative analysis of the performance of spatial interpolation methods for rainfall estimation using commercial microwave links. *J. Hydrometeorol.*, **22**, 831–843, <https://doi.org/10.1175/JHM-D-20-0164.1>.
- , P. Alpert, and H. Messer, 2022: Estimating the parameters of the spatial autocorrelation of rainfall fields by measurements from commercial microwave links. *IEEE Trans. Geosci. Remote Sens.*, **60**, 2004411, <https://doi.org/10.1109/TGRS.2022.3165309>.
- Fencl, M., J. Rieckermann, P. Šykora, D. Stránský, and V. Bareš, 2014: Commercial microwave links instead of rain gauges: Fiction or reality? *Water Sci. Technol.*, **71**, 31–37, <https://doi.org/10.2166/wst.2014.466>.
- Fischer, E. M., and R. Knutti, 2015: Anthropogenic contribution to global occurrence of heavy-precipitation and high-temperature extremes. *Nat. Climate Change*, **5**, 560–564, <https://doi.org/10.1038/nclimate2617>.
- Gleixner, S., T. Demissie, and G. T. Diro, 2020: Did ERA5 improve temperature and precipitation reanalysis over East Africa? *Atmosphere*, **11**, 996, <https://doi.org/10.3390/atmos11090996>.
- Graf, M., C. Chwala, J. Polz, and H. Kunstmann, 2020: Rainfall estimation from a German-wide commercial microwave link network: Optimized processing and validation for 1 year of data. *Hydrol. Earth Syst. Sci.*, **24**, 2931–2950, <https://doi.org/10.5194/hess-24-2931-2020>.
- Hersbach, H., and Coauthors, 2020: The ERA5 global reanalysis. *Quart. J. Roy. Meteor. Soc.*, **146**, 1999–2049, <https://doi.org/10.1002/qj.3803>.
- Huffman, G. J., and Coauthors, 2018: NASA Global Precipitation Measurement (GPM) Integrated Multi-satellite Retrievals for GPM (IMERG). Algorithm Theoretical Basis Doc., version 5.2, 35 pp., [https://gpm.nasa.gov/sites/default/files/document\\_files/IMERG\\_ATBD\\_V5.2.pdf](https://gpm.nasa.gov/sites/default/files/document_files/IMERG_ATBD_V5.2.pdf).
- ITU-R, 2005: P.838: Specific attenuation model for rain for use in prediction methods (Recommendation P.838-3). ITU-R, <https://www.itu.int/rec/R-REC-P.838-3-200503-I/en>.
- Kidd, C., G. Huffman, V. Maggioni, P. Chambon, and R. Oki, 2021: The global satellite precipitation constellation: Current status and future requirements. *Bull. Amer. Meteor. Soc.*, **102**, E1844–E1861, <https://doi.org/10.1175/BAMS-D-20-0299.1>.
- Kumah, K. K., J. C. B. Hoedjes, N. David, B. H. P. Maathuis, H. O. Gao, and B. Z. Su, 2021: The MSG technique: Improving commercial microwave link rainfall intensity by using rain area detection from Meteosat Second Generation. *Remote Sens.*, **13**, 3274, <https://doi.org/10.3390/rs13163274>.
- , B. H. P. Maathuis, J. C. B. Hoedjes, and Z. Su, 2022: Near real-time estimation of high spatiotemporal resolution rainfall from cloud top properties of the MSG satellite and commercial microwave link rainfall intensities. *Atmos. Res.*, **279**, 106357, <https://doi.org/10.1016/j.atmosres.2022.106357>.
- Leijnse, H., R. Uijlenhoet, and J. N. M. Stricker, 2007: Rainfall measurement using radio links from cellular communication networks. *Water Resour. Res.*, **43**, W03201, <https://doi.org/10.1029/2006WR005631>.
- , —, and —, 2008: Microwave link rainfall estimation: Effects of link length and frequency, temporal sampling, power resolution, and wet antenna attenuation. *Adv. Water Resour.*, **31**, 1481–1493, <https://doi.org/10.1016/j.advwatres.2008.03.004>.
- Leinonen, J., 2014: High-level interface to *T*-matrix scattering calculations: Architecture, capabilities and limitations. *Opt. Express*, **22**, 1655–1660, <https://doi.org/10.1364/OE.22.001655>.
- Maggioni, V., P. C. Meyers, and M. D. Robinson, 2016: A review of merged high-resolution satellite precipitation product accuracy during the Tropical Rainfall Measuring Mission (TRMM) era. *J. Hydrometeorol.*, **17**, 1101–1117, <https://doi.org/10.1175/JHM-D-15-0190.1>.
- Maranan, M., A. H. Fink, P. Knippertz, L. K. Amekudzi, W. A. Atiah, and M. Stengel, 2020: A process-based validation of GPM IMERG and its sources using a mesoscale rain gauge network in the West African forest zone. *J. Hydrometeorol.*, **21**, 729–749, <https://doi.org/10.1175/JHM-D-19-0257.1>.
- Messer, H., A. Zinevich, and P. Alpert, 2006: Environmental monitoring by wireless communication networks. *Science*, **312**, 713, <https://doi.org/10.1126/science.1120034>.
- Mishchenko, M. I., L. D. Travis, and D. W. Mackowski, 1996: *T*-matrix computations of light scattering by nonspherical particles: A review. *J. Quant. Spectrosc. Radiat. Transf.*, **55**, 535–575, [https://doi.org/10.1016/0022-4073\(96\)00002-7](https://doi.org/10.1016/0022-4073(96)00002-7).
- Moumouni, S., M. Gosset, and E. Houngninou, 2008: Main features of rain drop size distributions observed in Benin, West Africa, with optical disdrometers. *Geophys. Res. Lett.*, **35**, L23807, <https://doi.org/10.1029/2008GL035755>.
- Ostrometzky, J., and H. Messer, 2018: Dynamic determination of the baseline level in microwave links for rain monitoring from minimum attenuation values. *IEEE J. Sel. Top. Appl. Earth Obs. Remote Sens.*, **11**, 24–33, <https://doi.org/10.1109/JSTARS.2017.2752902>.
- Ouedraogo, W. Y. S. B., M. Djibo, A. Doumounia, S. R. Sanou, M. Sawadogo, I. Guira, and F. Zougmore, 2022: Rain events detection using energy variation of commercial microwave links attenuation. *Amer. J. Appl. Sci.*, **19**, 78–83, <https://doi.org/10.3844/ajassp.2022.78.83>.
- Overeem, A., H. Leijnse, and R. Uijlenhoet, 2013: Country-wide rainfall maps from cellular communication networks. *Proc. Natl. Acad. Sci. USA*, **110**, 2741–2745, <https://doi.org/10.1073/pnas.1217961110>.
- , —, and —, 2016a: Retrieval algorithm for rainfall mapping from microwave links in a cellular communication network. *Atmos. Meas. Tech.*, **9**, 2425–2444, <https://doi.org/10.5194/amt-9-2425-2016>.
- , —, and —, 2016b: Two and a half years of country-wide rainfall maps using radio links from commercial cellular telecommunication networks. *Water Resour. Res.*, **52**, 8039–8065, <https://doi.org/10.1002/2016WR019412>.
- , —, T. C. Leth, L. Bogerd, J. Priebe, D. Tricarico, A. Droste, and R. Uijlenhoet, 2021: Tropical rainfall monitoring with commercial microwave links in Sri Lanka. *Environ. Res. Lett.*, **16**, 074058, <https://doi.org/10.1088/1748-9326/ac0fa6>.
- Pastorek, J., M. Fencl, J. Rieckermann, and V. Bareš, 2022: Precipitation estimates from commercial microwave links: Practical approaches to wet-antenna correction. *IEEE Trans. Geosci. Remote Sens.*, **60**, 4104409, <https://doi.org/10.1109/TGRS.2021.3110004>.

- Polz, J., C. Chwala, M. Graf, and H. Kunstmann, 2020: Rain event detection in commercial microwave link attenuation data using convolutional neural networks. *Atmos. Meas. Tech.*, **13**, 3835–3853, <https://doi.org/10.5194/amt-13-3835-2020>.
- Pribe, J., and L. Panos, 2023: Enabling climate services through mobile network operator data. GSMA AgriTec. Tech. Rep., 66 pp., <https://www.gsma.com/mobilefordevelopment/resources/enabling-climate-services-through-mobile-network-operator-data/>.
- Rios Gaona, M. F., A. Overeem, A. M. Brasjen, J. F. Meirink, H. Leijnse, and R. Uijlenhoet, 2017: Evaluation of rainfall products derived from satellites and microwave links for the Netherlands. *IEEE Trans. Geosci. Remote Sens.*, **55**, 6849–6859, <https://doi.org/10.1109/TGRS.2017.2735439>.
- Schleiss, M., and A. Berne, 2010: Identification of dry and rainy periods using telecommunication microwave links. *IEEE Geosci. Remote Sens. Lett.*, **7**, 611–615, <https://doi.org/10.1109/LGRS.2010.2043052>.
- , J. Rieckermann, and A. Berne, 2013: Quantification and modeling of wet-antenna attenuation for commercial microwave links. *IEEE Geosci. Remote Sens. Lett.*, **10**, 1195–1199, <https://doi.org/10.1109/LGRS.2012.2236074>.
- Tomalka, J., and Coauthors, 2021: Representative concentration pathways – Climate risk profile Sahel region. UNHCR Tech. Rep., 20 pp., <https://www.unhcr.org/publications/brochures/61a49df44/representative-concentration-pathways-climate-risk-profile-sahel-region.html>.
- Turko, M., M. Gosset, M. Kacou, C. Bouvier, N. Chahinian, A. Boone, and M. Alcoba, 2021: Rainfall measurement from commercial microwave links for urban hydrology in Africa: A simulation framework for sensitivity analysis. *J. Hydrometeorol.*, **22**, 1819–1834, <https://doi.org/10.1175/JHM-D-20-0163.1>.
- Uijlenhoet, R., A. Overeem, and H. Leijnse, 2018: Opportunistic remote sensing of rainfall using microwave links from cellular communication networks. *Wiley Interdiscip. Rev.: Water*, **5**, e1289, <https://doi.org/10.1002/wat2.1289>.
- UNFCCC, 2022: Sharm el-Sheikh implementation plan. Revised draft decision -/CMA.4. UNFCCC, <https://unfccc.int/documents/621908>.
- van de Beek, R. C. Z., J. Olsson, and J. Andersson, 2020: Optimal grid resolution for precipitation maps from commercial microwave link networks. *Adv. Sci. Res.*, **17**, 79–85, <https://doi.org/10.5194/asr-17-79-2020>.
- van het Schip, T. I., A. Overeem, H. Leijnse, R. Uijlenhoet, J. F. Meirink, and A. J. van Delden, 2017: Rainfall measurement using cell phone links: Classification of wet and dry periods using geostationary satellites. *Hydrol. Sci. J.*, **62**, 1343–1353, <https://doi.org/10.1080/02626667.2017.1329588>.
- Vischel, T., G. Quantin, T. Lebel, J. Viarre, M. Gosset, F. Caze- nave, and G. Panthou, 2011: Generation of high-resolution rain fields in West Africa: Evaluation of dynamic interpolation methods. *J. Hydrometeorol.*, **12**, 1465–1482, <https://doi.org/10.1175/JHM-D-10-05015.1>.
- Wang, Z., M. Schleiss, J. Jaffrain, A. Berne, and J. Rieckermann, 2012: Using Markov switching models to infer dry and rainy periods from telecommunication microwave link signals. *Atmos. Meas. Tech.*, **5**, 1847–1859, <https://doi.org/10.5194/amt-5-1847-2012>.
- Zinevich, A., H. Messer, and P. Alpert, 2010: Prediction of rainfall intensity measurement errors using commercial microwave communication links. *Atmos. Meas. Tech.*, **3**, 1385–1402, <https://doi.org/10.5194/amt-3-1385-2010>.